ORIGINAL PAPER

Water-induced weakening retrogressive landslides: a study on the progressive failure process and formation mechanism of trailing edge fracture surfaces

Lijuan Sun[1] **· Fangming Shen**[1] **· Chenjia Li**[1]

Abstract

To study the formation mechanism of trailing edge fracture surfaces of retrogressive landslides, model tests, theoretical analysis, and numerical simulations are used. Firstly, a test device that could realize segmented softening of sliding zone soils was developed, and the progressive failure process was realized by injecting water into different permeable boxes. Twelve groups of model tests were carried out to observe the characteristics of the trailing edge cracks and the inclination angles of the fracture surfaces. The results showed that the longer the unstable sliding zone, the larger the deformation range of the slope. Different unstable sliding sections corresponded to a single main crack. The trailing edge cracks were mainly folded line type, (inverted) arc type, and linear type, and the folded line type cracks accounted for more than 1/2 of the total number. The inclination angles of the trailing edge fracture surfaces were mostly less than 90°, accounting for about 83.72% of the total. The inclination angles of the trailing edge fracture surfaces obtained by the sliding tensile cracking mechanism were the closest to the experimental values, and the relative errors were less than 10%. The formation mechanism of the trailing edge fracture surfaces is that tensile failure plays a leading role in the formation of the trailing edge fracture surfaces. The surface layer of the landslide body mainly undergoes tensile failure, and the middle and lower parts of the landslide body form a tensile-shear mixed action zone. The bottom sliding surface is dominated by shear failure.

Keywords Water-induced weakening · Retrogressive landslide · Trailing edge fracture surface · Formation mechanism · Progressive failure

Introduction

Landslide geological disasters are widely distributed worldwide and have great harm (Ding et al. 2012; Liu and Li 2015; Take et al. 2015; Xu et al. 2017; Graber et al. 2021). As an important landslide form, a retrogressive landslide is very common in engineering construction. Under the action of natural and human factors such as reservoir water rise, rainwater erosion, valley cutting, and engineering excavation, the slope toe loses support and the internal stress field changes. It is easy to form cracks at the trailing edge and gradually develop backward, forming retrogressive landslides (Qi et al. 2018; Kennedy et al. 2021; Shan et al. 2021).

Among the various factors inducing retrogressive landslides, rainfall (Alimohammadlou et al. 2014; Zhang et al. 2016; Pan et al. 2017), reservoir water level change (Liu et al. 2021), groundwater rise (Lv et al. 2019), and irrigation (Lian et al. 2020; Graber et al. 2021) will lead to the first saturation weakening of soil at the foot of the slope, causing retrogressive sliding of the slope and forming retrogressive landslides. Such cases have been reported many times (Oezdemir and Delikanli 2009; Huang et al. 2018; Yin et al. 2020). According to statistics, among the many factors inducing landslides, rainfall and reservoir water account for the vast majority (Guo et al. 2020; Huang et al. 2020). Figures 1 and 2 show the progressively upward retrogressive landslides induced by river erosions toe and rainfall infiltrations into the sliding zone soils, respectively. Therefore, the study of water-induced weakening retrogressive landslides has important practical significance.

Figure 3 is the schematic diagram of a retrogressive landslide caused by water saturation weakening of the sliding

✉ Lijuan Sun
  sunlijuan@jlju.edu.cn

1 School of Transportation Science and Engineering, Jilin Jianzhu University, Changchun, Jilin 130118, China

Fig. 1 A reservoir water weakening-induced retrogressive landslide (Eshraghian et al. 2008)
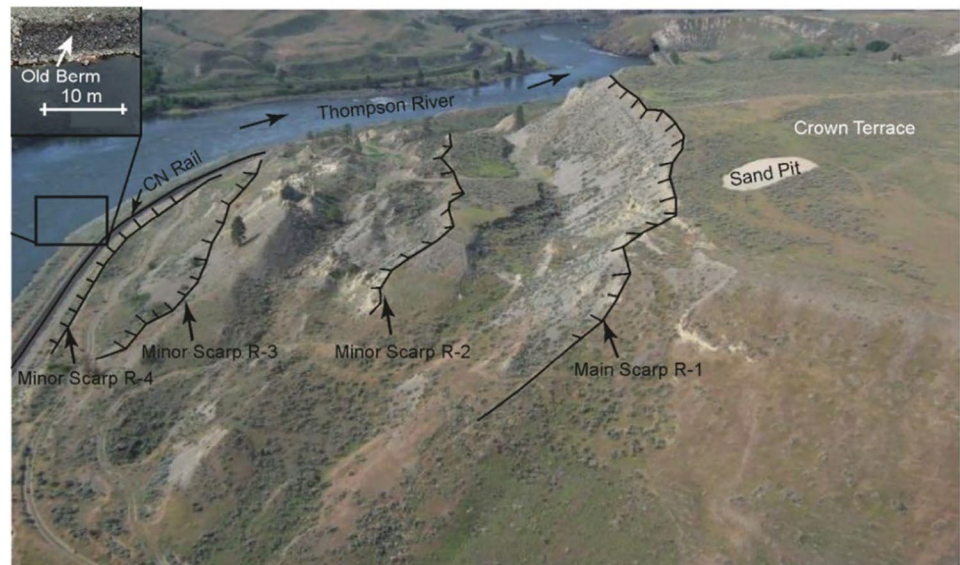
zone soil. Generally, factors such as rainfall, reservoir water, irrigation, and groundwater will cause the sliding zone soil at the low position to reach saturation first, soften the soil, and reduce the shear strength, resulting in the destroying of the local slope body. With the continuous expansion of the water-saturated range of the sliding zone soil, the whole slope instability is finally induced (Jiang et al. 2014; Wang et al. 2020; Liao et al. 2021).

The natural slope often causes retrogressive sliding due to the river valley cutting or soaking the foot of the slope, forming a multi-stage trailing edge fracture surfaces. In Fig. 4, the "Scrap1," "Scrap2," and "Scrap3" are the trailing edge

fracture surfaces formed during the graded sliding process of retrogressive landslides (Kennedy et al. 2021). However, the instability sliding of the sliding masses at all levels does not occur instantaneously, but has the characteristics of progressive failure. In 1964, Skempton (1964) proposed the concept of progressive failure of the slopes and pointed out that the phenomenon of slope instability often does not reach the limit state at each point on the sliding surface at the same time, but begins to break from one part and then develops to other parts. After decades of development, the landslide has the characteristics of progressive failure, which has become a consensus in the landslide research community. The

Fig. 2 A rainwater weakening-induced retrogressive landslide (Oezdemir and Delikanli 2009)
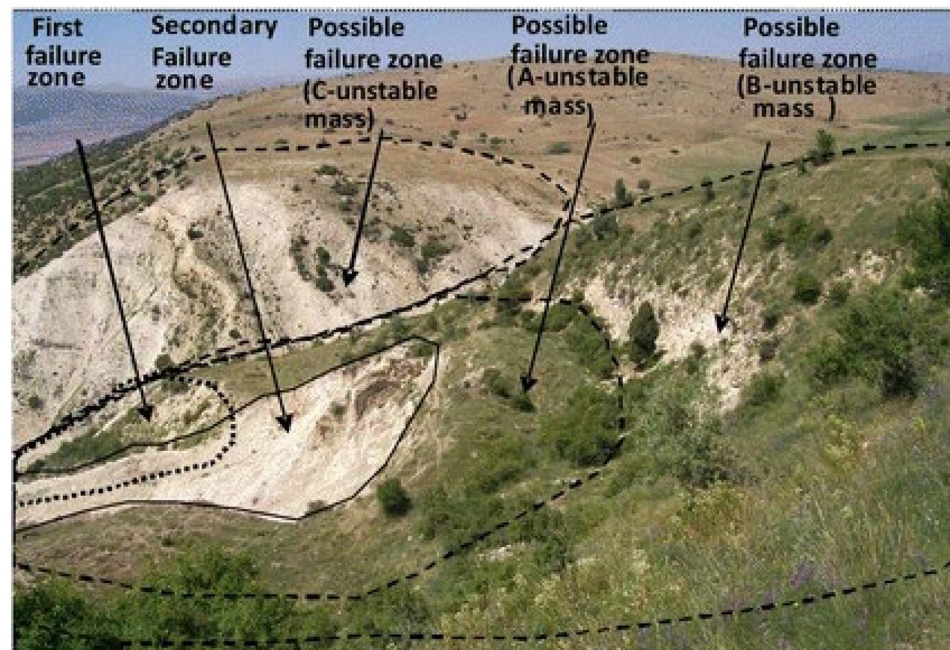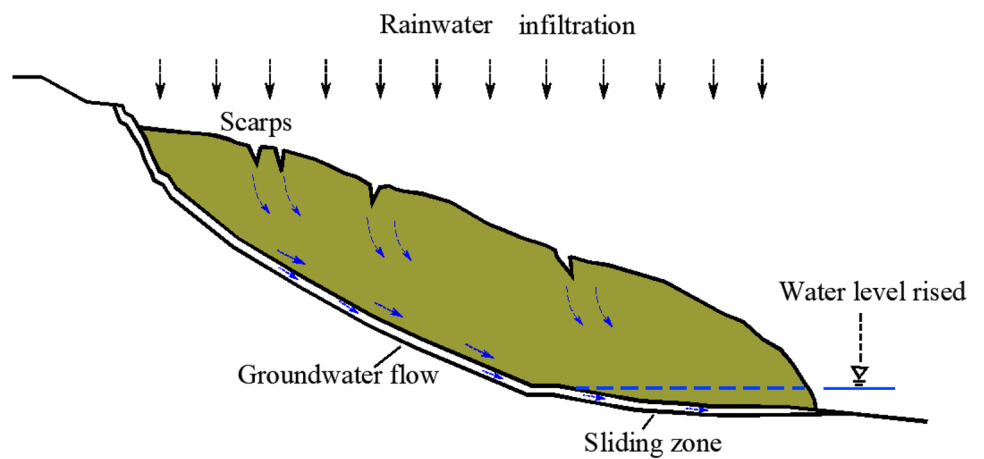
Fig. 3 Representation of water infiltration path and softening process of the sliding zone soil

revelation and application of the progressive failure law of landslides have also become a hot issue in landslide research (Troncone et al. 2015; Zhang et al. 2020; Zuo et al. 2021).

In the progressive failure process of retrogressive landslides, when each sliding mass loses stability, it forms a bottom sliding surface and trailing edge fracture surface (Sun et al. 2018), as shown in Fig. 4. Similar to the general landslide analysis, the primary task in the retrogressive landslide analysis is to carry out a landslide survey and determine the landslide scale (Sun et al. 2018). The core task is to determine the scope of the landslide, namely the spatial sliding surfaces and the trailing edge fracture surfaces. The bottom sliding surfaces can be obtained by drilling data analysis, such as the developed existing sliding surfaces or weak interlayers, their spatial positions are easy to determine. The trailing edge fracture surfaces are generally determined by slope cracks. However, the landslide scarps only reveal the surface boundary of landslide development. There is no reliable method for how the scarps extend into the slope and

intersect with the existing sliding surfaces (or weak interlayer). According to experience, the trailing edge is usually considered to be a fracture surface with a steep inclination angle (Xu et al. 2014; Sun et al. 2018). However, the values of the specific inclination angles have greater subjective randomness. In fact, the spatial shapes of the trailing edge surfaces determine the scale of the landslide body, which has an important influence on the stability analysis and thrust calculation of landslides. Therefore, it is necessary to study the progressive failure process and formation mechanism of the trailing edge fracture surfaces of retrogressive landslides.

The indoor model test is an essential means for studying the progressive failure process and formation mechanism of retrogressive landslides. Previous studies primarily used slope rainfall or reservoir water soaking slope to study the landslide instability mechanism, but these test methods were difficult to infiltrate into the sliding zone in a short time. In most cases, the shallow slope surface has been scoured and destroyed, but the sliding zone soils have not yet reached

Fig. 4 Multiple sliding masses and multiple scarps caused by water-induced weakening retrogressive landslides. SM represents sliding mass
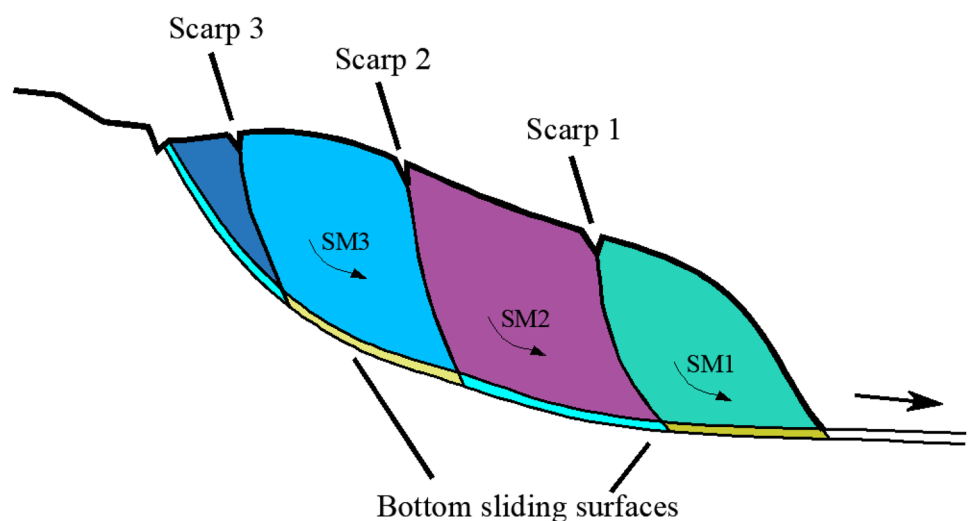
saturation, and such landslides are not caused by sliding zone instability (Regmi et al. 2014; Yin et al. 2020). However, for the water-induced weakening retrogressive landslides, the saturated simulation of the sliding zone soils is more realistic than the saturated simulation of the slope body. For this reason, a model test device that can simulate the segmental instability is designed and developed in this paper. Water can be injected into different segmented bottom sliding surfaces to achieve graded softening of sliding zone soils and reproduce the progressive failure process of retrogressive landslides.

In addition, many scholars have used the finite element software and discrete element software to discuss the formation process of retrogressive landslides on the study of landslide instability mechanism. In terms of finite element analysis, Kaya et al. (2016) used the Phase2 finite element program to determine the strength reduction factor (SRF) of the slope. It was considered that the failure mechanism is not directly controlled by joints, which may be related to the lower strength parameters of rock mass and joints, and the preventive measures to stabilize the region by using the Phase2 program were used. Su et al. (2019) proposed a landslide sliding distance prediction model. The sliding surface parameters were derived by the Bishop method, and the predicted landslide distance was very close to the measured value. Li et al. (2022) used Phase2 and Optum G2 numerical programs based on strength reduction finite element analysis and finite element limit analysis methods respectively for numerical analysis. It was considered that the failure mechanism of slope toe was the dominant failure mechanism, and the depth of the failure surface was more sensitive to the change of slope angles, cohesion, and water level position. In terms of discrete element analysis, such as Wei et al. (2019) combined with a digital elevation model (DEM), a PFC three-dimensional numerical model of the landslide was constructed to simulate the failure process of the slope. The simulation results were in good agreement with the real landslide characteristics and the video interpretation of the landslide movement process. Chang et al. (2022) developed a particle flow code (PFC) to simulate the failure process of loess landslides under strong earthquakes. Hu et al. (2022) used the PFC numerical model to invert the digital elevation model and shear strength parameters corresponding to the rheology of landslide debris flow materials. The simulation results were consistent with the shape of the landslide dam. However, there is no research on the formation mechanism of the trailing edge fracture surfaces. Therefore, this paper will focus on the formation mechanism of the trailing edge fracture surfaces of retrogressive landslides.

Based on the above analysis, this paper taked the water-induced weakening retrogressive landslides as the research object and designed a test device that could simultaneously simulate the softening effect of groundwater on the sliding zone soils and the progressive failure process of retrogressive landslides. The device consisted of several permeable boxes to form a segmented sliding surface, which could simulate the sliding surfaces of various geometric shapes. By injecting water into different permeable boxes, the sliding zone soils were softened in stages to simulate various landslide failure modes. Twelve test schemes were designed to simulate the instability of different sliding zone soils, sliding zone shapes, slope angles, and slope thicknesses, and to observe the inclination angles of the trailing edge fracture surfaces of the unstable sliding mass. Finally, the forming mechanism of the trailing edge fracture surfaces of retrogressive landslides was discussed by the finite element method and discrete element method.

Model tests

"Segmented sliding surface bottom infiltration method" test device

Studies have shown that rainfall and reservoir water are the main factors inducing landslide revival. The reasons include the increase of landslide weight caused by rainfall, the erosion of the slope surface caused by reservoir water rising, the saturated softening of the sliding zone soils, and the seepage outside the slope caused by the groundwater level rising. Among them, the infiltration of surface water or groundwater into the potential sliding zone leads to a decrease in the shear strength of sliding zone soils, which is the main reason for the instability of landslides. For retrogressive landslides, the action process of the water-saturated weakening develops gradually, and the instability of the landslides is a typical progressive failure process. Therefore, for the sliding simulation of water-induced weakening retrogressive landslides, it is necessary to simultaneously reflect the softening effect of groundwater on the sliding zone soils and the progressive failure characteristics of retrogressive landslides.

The existing model tests generally simulate the influence of groundwater on the stability of landslides by rainfall on the slope or setting reservoir water, which is difficult to ensure the uniform infiltration of rainwater or reservoir water into the sliding zone soils. In most cases, the shallow layer of the slope has been scoured and destroyed, but the sliding zone soils has not yet reached saturation. Therefore, there is still a lack of suitable test methods for the simulation of the progressive failure process of water-induced weakening retrogressive landslides. To this end, a new test device is developed to simulate the gradual saturation softening process of the sliding zone soils and the gradual instability process of retrogressive landslides, to reflect the main sliding factors of the gradual instability of retrogressive landslides, as shown in Fig. 5.
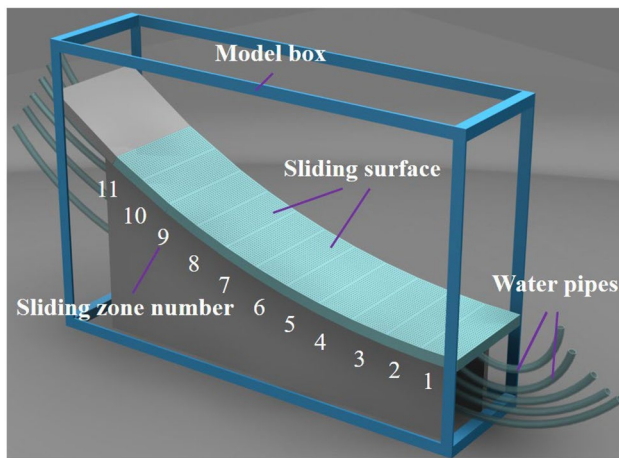
Fig. 5 "Segmented sliding surface bottom infiltration method" test device (Sun et al. 2018)

In order to realize the model test function and meet the test requirements, the test device was mainly composed of a model box, permeability system, water injection system, test system, and high-speed photography acquisition. To facilitate the observation of the deformation and development process of landslides, transparent tempered glass was used as the visual window on both sides of the model box and transparent coordinate calibration paper (used for accurate deformation positioning analysis) was set. Through the video tracker and digital camera installed on the sides of the model box, the whole process of deformation characteristics and cracks development of the sliding masses could be observed in real time. The size of the model box was 120 cm × 30 cm × 80 cm (length × width × height). The model box was used to fill the sliding mass soils and the sliding zone soils, and the sliding bed was fixed. The main body of the device was a segmented sliding surface composed of several permeable boxes, as shown in Fig. 5. The shapes of the sliding zone could be changed by changing the shapes of the sliding bed, such as simulating arc sliding zone, folded line sliding zone, and linear sliding zone. The size of the permeable box was 30 cm × 12 cm × 2 cm, which was made of a 1-mm thick steel plate. The permeable box was empty except for a 1-cm-high bracket. The permeable stones were placed on the bracket, and the permeability coefficient of the permeable stones was 1×10^{-3} cm/s. The water injection pipes were drawn from the bottom of the permeable boxes, and each group of water injection pipes was set to the same head and connected with the water injection container. At the same time, the water control ball valves were installed on the upper part of the water injection pipes to control the opening and closing of water and adjust the flow rate.

At the beginning of the test, the sliding zone soils and sliding mass soils were filled successively above the segmented sliding surface. The water injection pipes of each group were adjusted to the same flow rate, and the water flowed through the permeable stones and infiltrated evenly into the sliding zone soils. The sliding zone soils softened with the increase of water injection to realize the graded instability of sliding masses. Twelve groups of schemes were designed. By injecting water into different permeable boxes from front to back, various segmented sliding and progressive instability processes of retrogressive landslides could be simulated.

Test model

In the experiment, 50-mesh silica sand and 600-mesh ultrafine clay were used as raw materials to configure the sliding zone soils and sliding mass soils. The mass ratio of silica sand to ultrafine clay in sliding mass soils was 2:1, and the sliding zone soils were composed of ultrafine clay. Twelve groups of test schemes were designed, mainly considering the effects of different instability sliding zone lengths, sliding zone shapes, slope angles, and sliding mass thickness on the trailing edge morphology of retrogressive landslides. The slope model was shown in Fig. 6. The permeable boxes were numbered from the front shear outlet of the model boxes, which were 1, 2, and 3… 11 from front to back. The design of working conditions was shown in Table 1.

The physical and mechanical parameters including sliding mass soils and sliding zone soils were shown in Table 2. Among them, γ was the natural weight, E_s was the compression modulus, c was the cohesion, and φ was the internal friction angle. The permeability coefficient of the slope material was $3 \sim 5 \times 10^{-6}$ m/s, which was sufficient to absorb all the seeping water. In the process of making the model, the permeable boxes were laid on the sliding zone in turn, and the joint and the surrounding boundary were sealed. Then, the glass plate of the model box was layered and lined, and the outline of the sliding mass was drawn. The sensors were arranged according to the experimental design. The sliding mass soils were compacted by layers and scratched between layers. After the laying was completed, the slope was cut to obtain the design slope. To reduce the friction between the slope and the glass on both sides, a friction reducer was added to the contact area to minimize the influence of side friction.

Description: No. 1 ~ No. 12 correspond to Fig. 6a ~ i, respectively. The data in each group in the table represent the parameters of sliding mass soils and sliding zone soils, for example, 16.14/12.15. The previous data represents sliding mass soils, and the latter represents sliding zone soils.

Fig. 6 Sketches of different schemes in physical model tests: **a**, **b**, and **c** show different schemes with various lengths of the softened sliding zone; **d**, **e**, and **f** show different schemes with various thickness of the sliding masses; **g**, **h**, and **i** show different schemes with various shapes of the sliding zone; **j**, **k**, and **l** show different cases with various slope angles
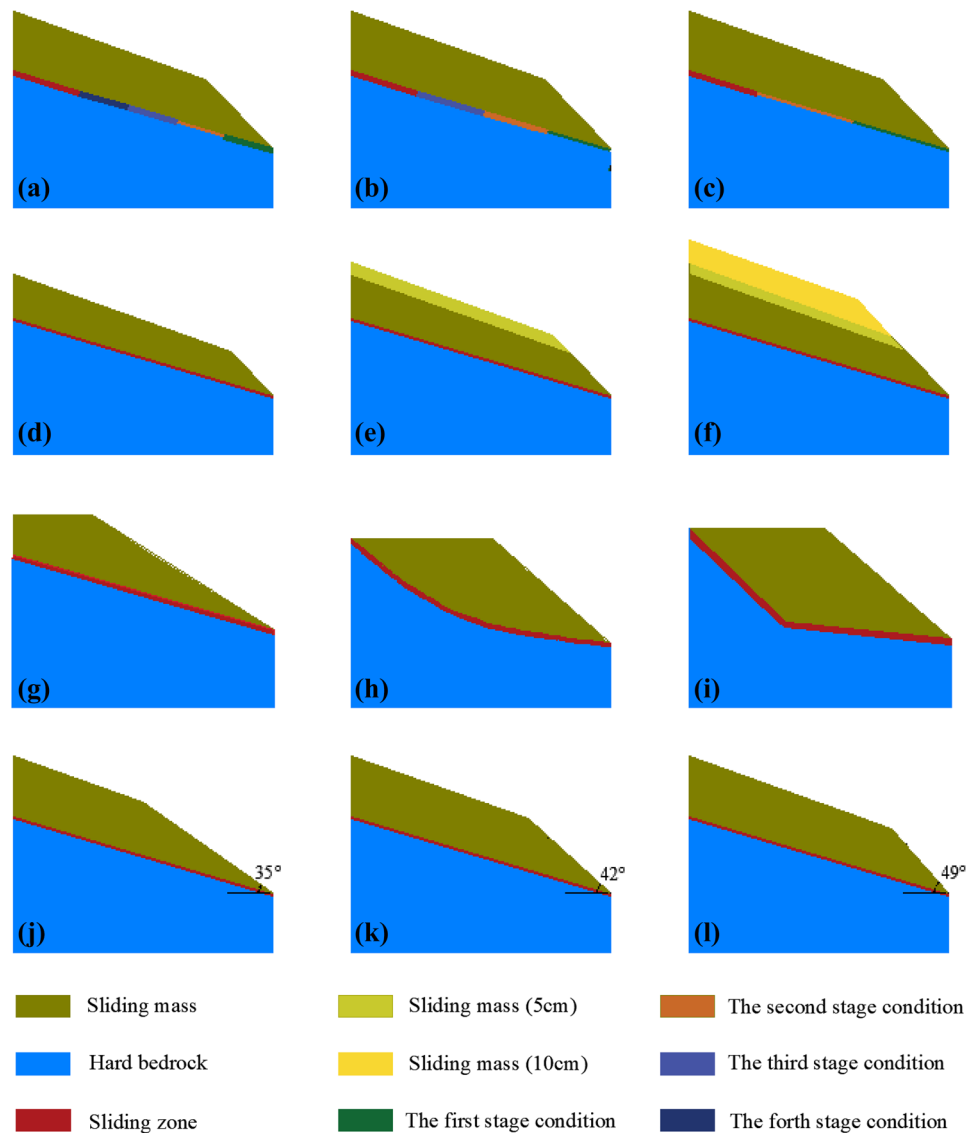

Table 1 Test schemes design

No	Sand-soil ratio		Slope shape		Sliding section (water injection condition) According to penetration box number)
	Sliding mass soil	Sliding zone soil	Sliding surface shape	Slope shape	
1	2:1	0:1	Linear type	Two-section line	2+3/4+5/6+7/8+9
2	2:1	0:1	Linear type	Two-section line	2+3+4/5+6+7/8+9+10
3	2:1	0:1	Linear type	Two-section line	2+3+4+5/6+7+8+9
4	2:1	0:1	Linear type	Two-section line	2+3/4+5/6+7/8+9
5	2:1	0:1	Linear type	Two-section line	2+3/4+5/6+7/8+9
6	2:1	0:1	Linear type	Two-section line	2+3/4+5/6+7/8+9
7	2:1	0:1	Linear type	Two-section line	2+3/4+5/6+7/8+9
8	2:1	0:1	Arc type	Two-section line	2+3+4/5+6+7/8+9
9	2:1	0:1	Fold type	Two-section line	2+3+4/5+6+7/8+9
10	2:1	0:1	Linear type	Two-section line	2+3+4/5+6+7/8+9
11	2:1	0:1	Linear type	Two-section line	2+3+4/5+6+7/8+9
12	2:1	0:1	Linear type	Two-section line	2+3+4/5+6+7/8+9

Table 2 Physical and mechanical parameters of model soil

| No	γ/kN/m³	e —	E_s/MPa	c/kPa	φ/°
1	16.14/12.15	0.76/1.05	8.45/4.12	11.18/40.92	32.88/18.80
2	15.60/11.78	0.80/1.14	7.56/4.58	16.00/43.14	21.42/18.76
3	14.26/10.87	0.98/1.17	8.57/4.54	15.08/40.37	26.60/18.81
4	15.34/10.08	0.85/1.12	7.45/4.31	13.63/40.14	23.37/17.66
5	15.07/11.31	0.88/1.17	7.68/4.27	14.16/41.37	25.55/18.24
6	13.18/12.24	1.18/1.22	8.96/5.31	15.33/43.11	24.68/17.64
7	14.26/11.24	0.97/1.15	7.98/5.24	12.83/40.47	30.38/16.25
8	13.74/10.36	1.13/1.18	8.02/7.64	11.45/12.23	20.19/19.78
9	14.75/13.54	0.97/1.15	8.24/8.17	12.34/10.38	18.66/20.05
10	15.02/11.32	0.89/1.13	7.34/4.57	10.55/41.03	18.46/17.46
11	15.28/10.54	0.88/1.24	8.47/5.01	12.34/41.13	20.66/18.38
12	16.71/11.29	0.76/1.15	8.16/4.25	16.57/44.18	20.03/15.87

Test process

The influence of water-saturated softening of the sliding zone soils of the trailing edge fracture surfaces of retrogressive landslides is mainly simulated in the experiment. Therefore, the cohesion and internal friction angles of the sliding zone soils under different water contents were tested before the experiment. Six groups of the sliding zone soils with water contents (10%, 15%, 20%, 25%, 30%, 35%) were configured, and the results were plotted as curves, as shown in Fig. 7. Figure 7 shows that with

the increase of water content, the cohesion, and internal friction angles of the sliding zone soils decrease significantly, and the shear strength of the sliding zone soils is controlled by the change of water content. To further prove the softening effect of water on the sliding zone soils, volumetric water content sensors were set up at the sliding zone of the model slope to monitor the real-time change trend of water content in sliding zone soils. The results showed that with the increase of the volumetric water content of the sliding zone soils, the deformation of the model slope gradually increased until it increased to about 35% ~ 40% and then tended to be stable (Sun et al. 2023).

At the beginning of the experiment, the sliding zone soils were softened in sections according to the design conditions. The sliding zone soils were gradually saturated, and the shear strength was continuously reduced. The unstable sliding masses gradually formed and slipped forward. With the continuous development of deformation, the sliding masses were gradually separated from the rear sliding masses. Due to the lack of support, the anti-sliding force of the rear sliding masses was reduced, and the stability was reduced to the limit equilibrium state. After that, small deformation began to occur until the former sliding masses gradually stabilized. At this time, the following working conditions were carried out. To avoid the potential corrosion of water on the sliding mass soils, the water injection rate was controlled in a small range. The sliding zone soils within the scope of the first group permeable boxes simultaneously injected with water was called the first-stage sliding zone, and the

Fig. 7 The $c \sim \omega/\varphi \sim \omega$ curves of the sliding zone soils
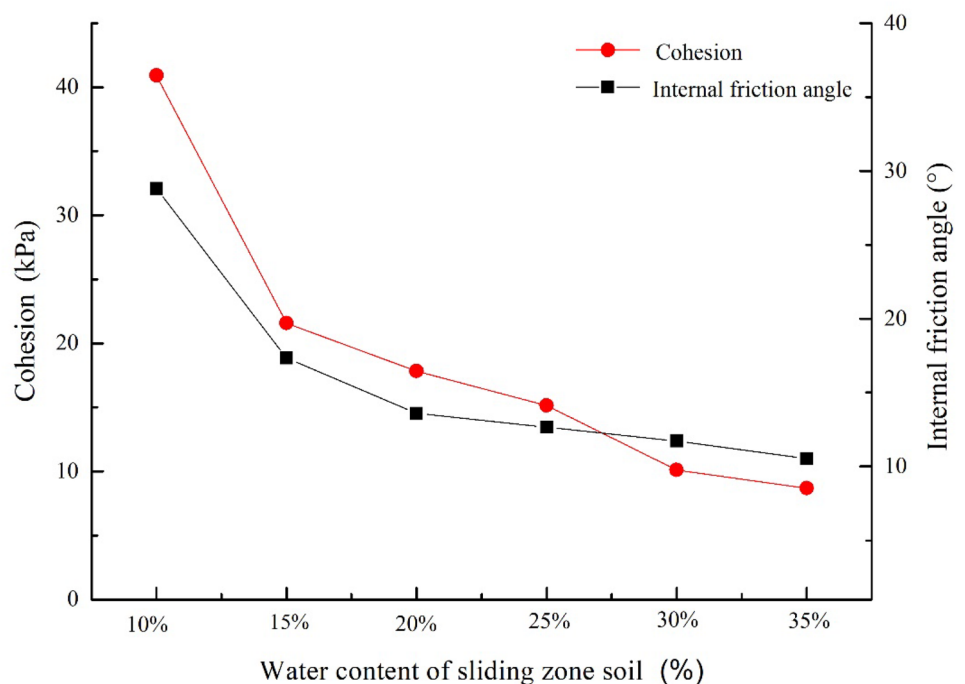
deformation slope caused by its softening was called the first-stage sliding mass, and so on.

Test result analysis

Evolution characteristics of trailing edge cracks

Based on the experimental phenomena of each group, the trailing edge crack morphology has the following typical development laws:

1. There was a good correlation between the length of the unstable sliding zone and the deformation range of the slope body. The longer the unstable the sliding zone, the more extensive the deformation range of the slope. The deformation of the sliding zone directly determined the deformation of the slope body, and the sliding zone controlled the stability of the slope body. Taking No. 8 as an example, crack1 was formed on the slope surface when water was injected into the first-stage sliding zone (permeable boxes 2~4), and the range of the deformed slope was called sliding mass 1 (SM1). When water was injected into the second-stage sliding zone (permeable boxes

5~7), crack2 was formed on the slope surface, and the range of the deformed slope was called sliding mass 2 (SM2). When water was injected into the third-stage sliding zone (permeable boxes 8~9), crack3 was formed on the slope surface, and the range of the deformed slope was called sliding mass 3 (SM3). The formation process of sliding masses at all levels was shown in Fig. 8.

2. The spatial forms of the trailing edge cracks in the landslides were not single, which were affected by various factors, mainly manifested as folded line, (inverted) arc, and linear. Among them, the folded line cracks accounted for more than 1/2 of the total number, as shown in Fig. 9.

3. Each unstable sliding section corresponded to a single crack. A certain section of the sliding zone was instability, and only one main crack was observed on the slope corresponding to it, as shown in Fig. 10a. Injecting water caused cracks on the slope surface, if the injected water volume increased, the width of original crack would continue to increase, which was equivalent to the main crack of the real landslides. Taking No. 7 and No. 9 as examples, they were divided into three sliding zones, namely the first-stage sliding zone (permeable boxes 2~4), the second-stage sliding zone (permeable

Fig. 8 The gradual development process of the trailing edge cracks
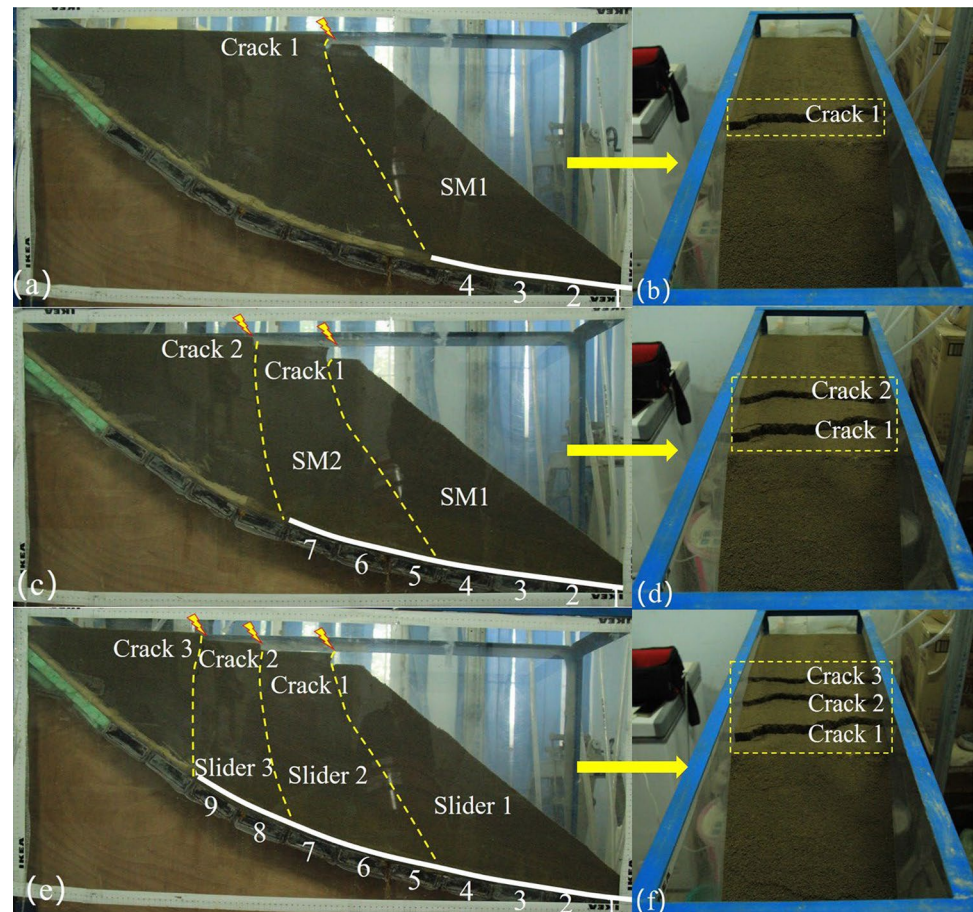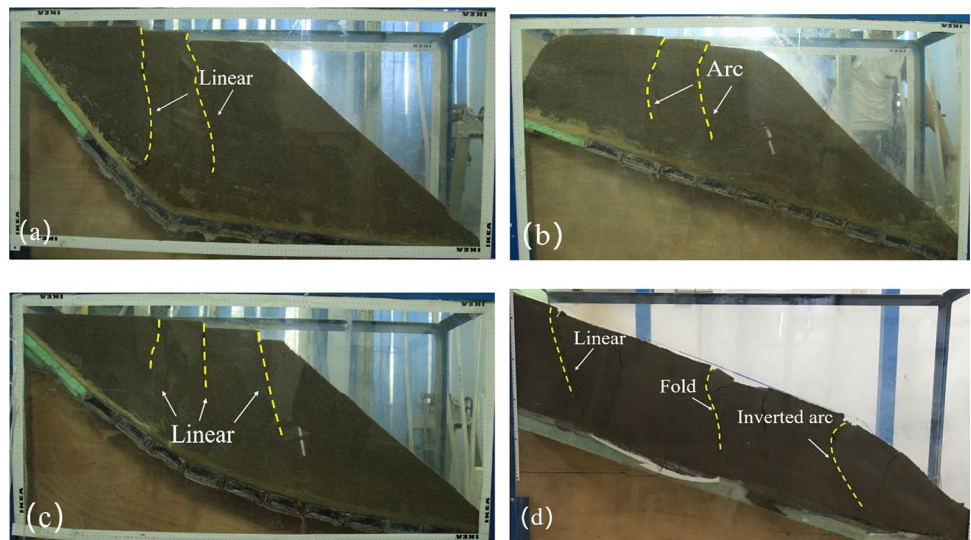
Fig. 9 The trailing edge crack morphology: **a**, **b**, **c**, and **d** show the cracks morphology of linear, arc, and fold, respectively

boxes 5~7), and the third-stage sliding zone (permeable boxes 8~9). Firstly, the first-stage sliding zone was injected with water, and the sliding zone soil was gradually saturated and softened, and then, a main crack appeared on the back slope of the permeable box 4, as shown in Figs. 10a~b and 11a~b; subsequently, water was injected into the second-stage sliding zone, and the second main crack (Figs. 10c~d, 11c~d) appeared on the slope above the permeable box 7; finally, the third main crack (Figs. 10e~f, 11e~f) was generated on the slope above the permeable box 9 by injecting water into the third-stage sliding zone.

4. The thickness of the slope affected the crack morphology of the trailing edge fracture surfaces. When the thickness was larger, the cracks in the trailing edge of the slope were "inverted arc"; when the thickness decreased and the trailing edge cracks developed into a "fold line", the final shape was the "straight + semi-arc" type, as shown in Fig. 12. The increase of slope thickness caused the change of slope stress state, which led to the stress concentration near the slope toe, so the high slope was unsafe.

5. The slope angle change of the model slope led to a significant change in the morphology of the trailing edge cracks. With the increase of the slope angles, the trailing edge cracks of the sliding masses at all levels gradually presented "L-shaped fold line", "linear type", "arc type", "inverted arc line", and "fold line". This change process showed that when the slope angles were small, the slope mainly underwent translational failure (Fig. 13a~b); as the angle increased, the rotation failure was gradually dominant (Fig. 13c). Finally, rotational failure and

translational failure occurred simultaneously (Fig. 13d) (Wang et al. 2016). The change of slope angles has a great influence on the stress field of the landslide body, thus forming different trailing edge crack forms.
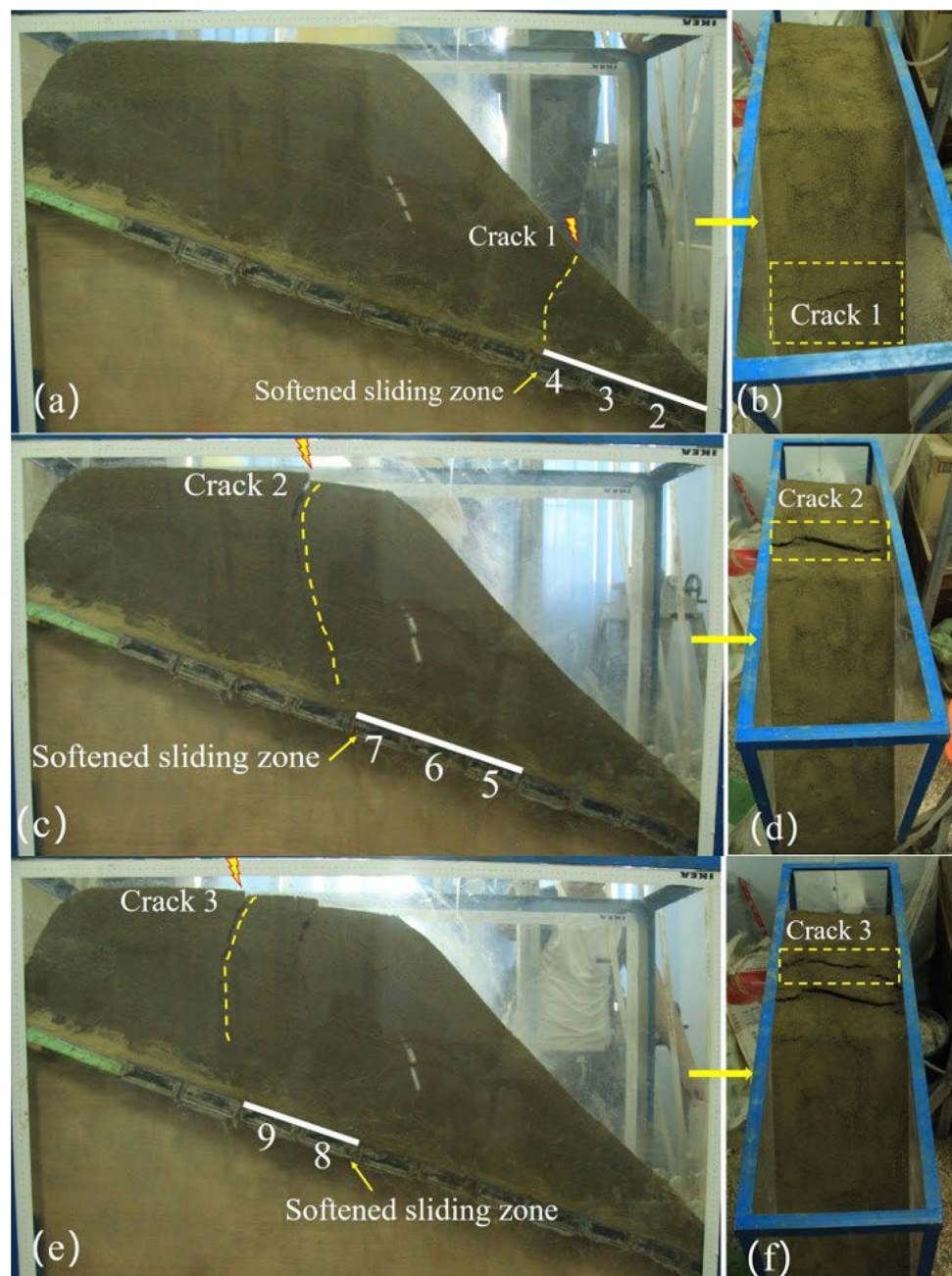
Inclination angles of the trailing edge fracture surfaces

Taking No. 8 as an example, the slope model before injecting water was shown in Fig. 14. To better quantify the shapes of the trailing edge fracture surfaces, the concept of the inclination angles of the trailing edge fracture surfaces was proposed. The inclination angle was the angle between the fracture point on the slope and the end line of the unstable sliding zone and the horizontal plane, as shown in Fig. 15. According to the scheme design, the sliding zone composed of permeable boxes was divided into three levels, and water was injected into the permeable boxes from front to back, forming three-stage trailing edge fracture surfaces, respectively. The inclination angles of the trailing edge fracture surfaces were measured, as shown in Fig. 16. According to this quantitative method, the inclination angles of the trailing edge fracture surfaces were summarized, as shown in Table 3.

GK_i represents the working conditions; the "2~3" represents the combination of permeable boxes 2 and 3; the "2~4" represents the combination of permeable boxes 2, 3, and 4; the others are the same.

The inclination angles of the trailing edge fracture surfaces of each group are analyzed, and the conclusions are as follows:

Fig. 10 The trailing edge crack morphology of each sliding zone instability (No. 7): **a**, **b** the first-stage sliding zone (permeable boxes 2~4); **c**, **d** the second-stage sliding zone (permeable boxes 5~7); **e**, **f** the third-stage sliding zone (permeable boxes 8~9)

1. The inclination angles of the trailing edge fracture surfaces were mostly steep inclination angles of less than 90°, accounting for about 83.72% of the total. The inclination angles within 60°~70°, 70°~80°, and 80°~90° were 6.98%, 34.88%, and 41.86%, respectively.

2. In the same test condition, the inclination angles of the trailing edge fracture surfaces were parallel to the straight slope with the same thickness. With the increase of slope thickness, the inclination angles of the trailing edge fracture surfaces gradually increased. The slope deformation range was about 1~1.5 times the length of the unstable sliding zone.

3. Different forms of sliding surfaces had a direct influence on the slope stress field. Therefore, different shapes of trailing edge cracks led to different inclination angles of trailing edge fracture surfaces. Due to the limited number of samples, no regular conclusion had been reached.

At present, the inclination angles of the trailing edge fracture surfaces are only connected by the position of the slope cracks and the end of the softened sliding zone. This simplified method is still insufficient and needs further exploration.

Fig. 11 The trailing edge crack morphology of each sliding zone instability (No. 9): **a**, **b** the first-stage sliding zone (permeable boxes 2 ~ 4); **c**, **d** the second-stage sliding zone (permeable boxes 5 ~ 7); **e**, **f** the third-stage sliding zone (permeable boxes 8 ~ 9)
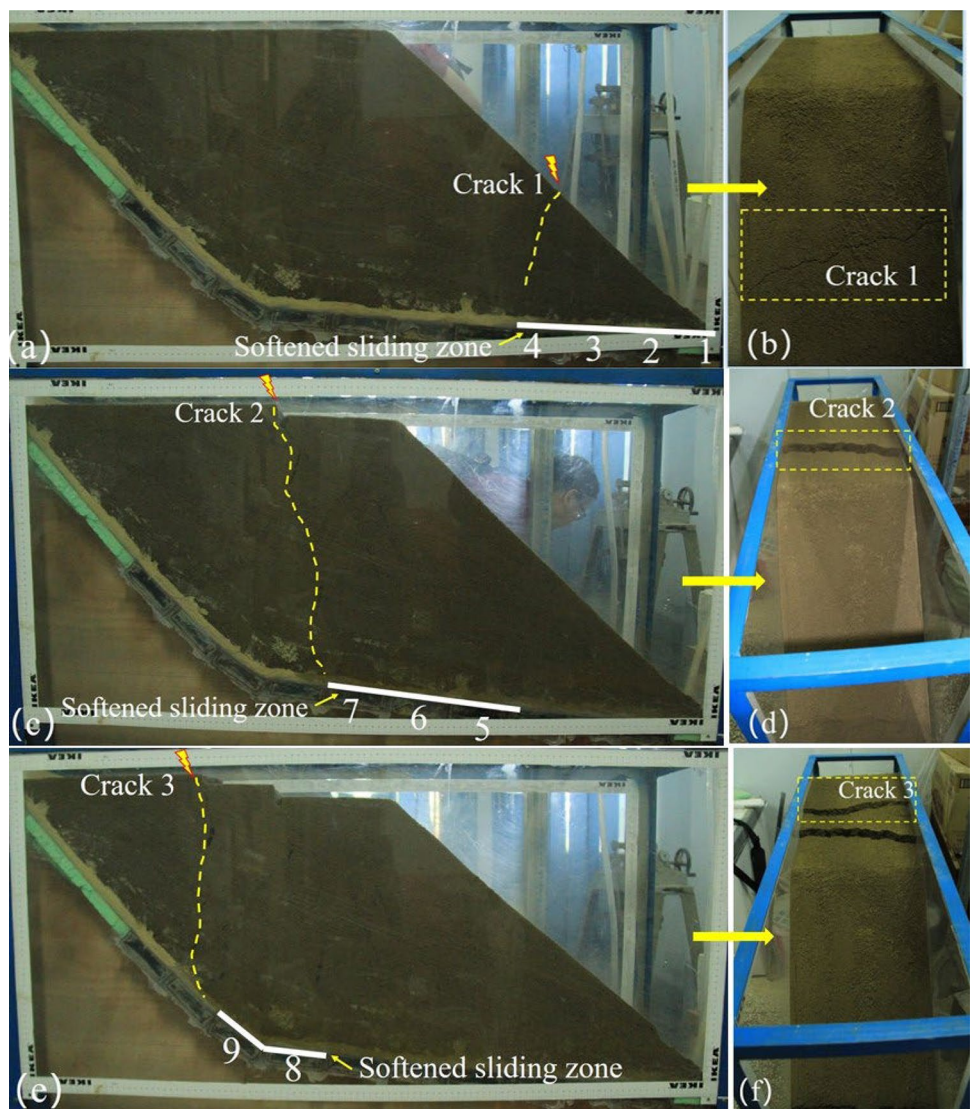

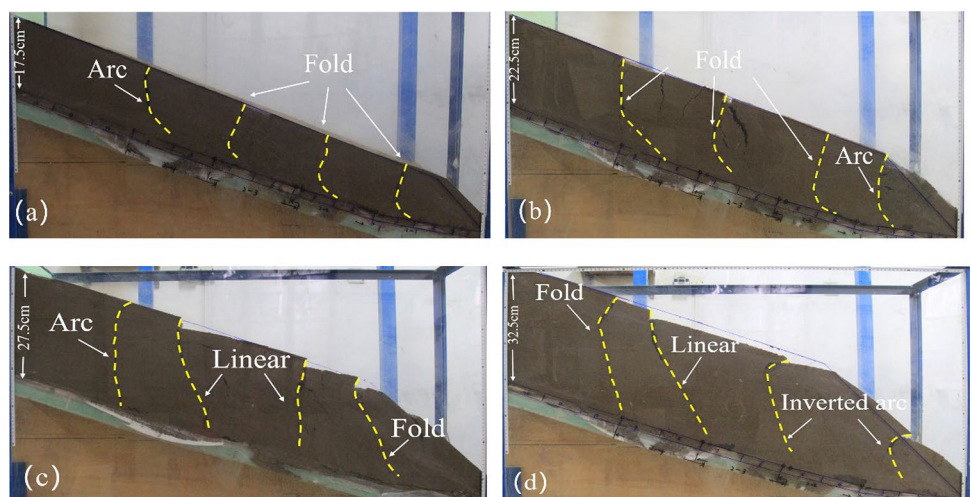**Fig. 12** Crack morphology of trailing edge fracture surfaces with different thickness

Fig. 13 Crack morphology of trailing edge fracture surfaces with different slope angles
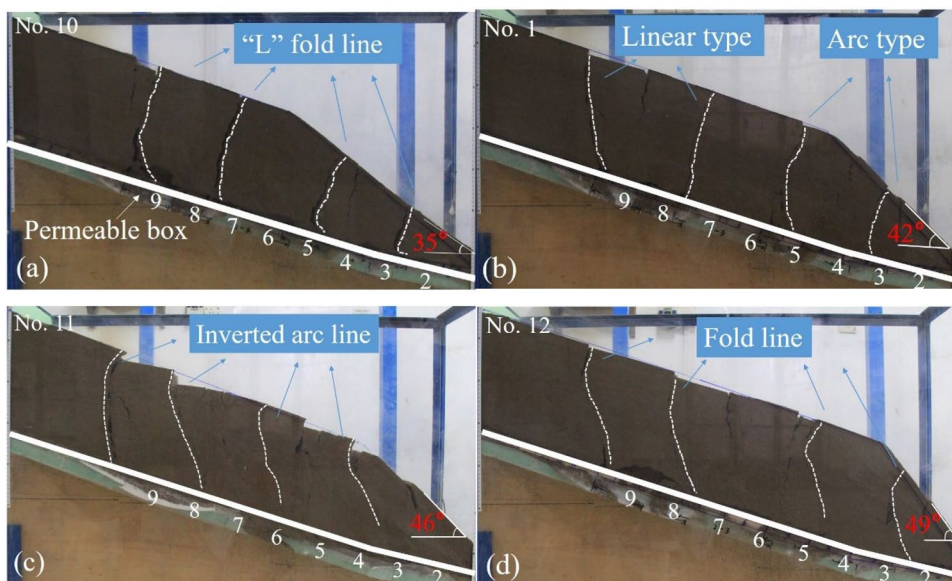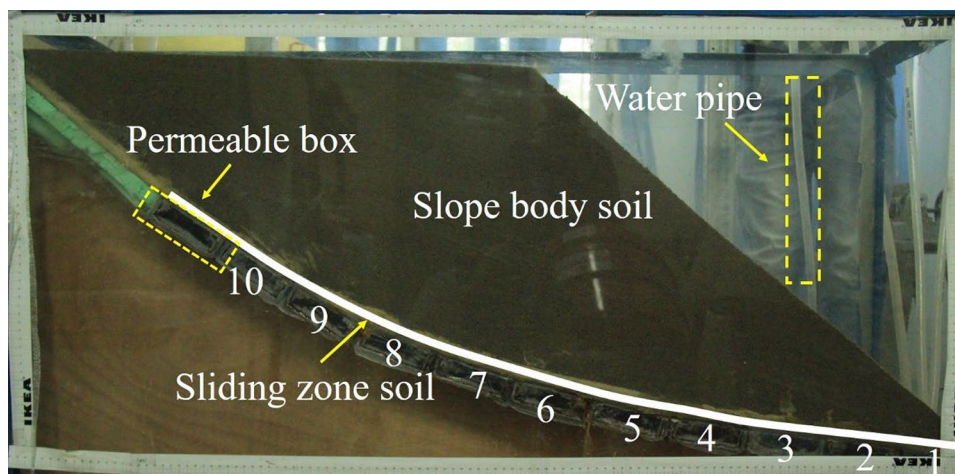

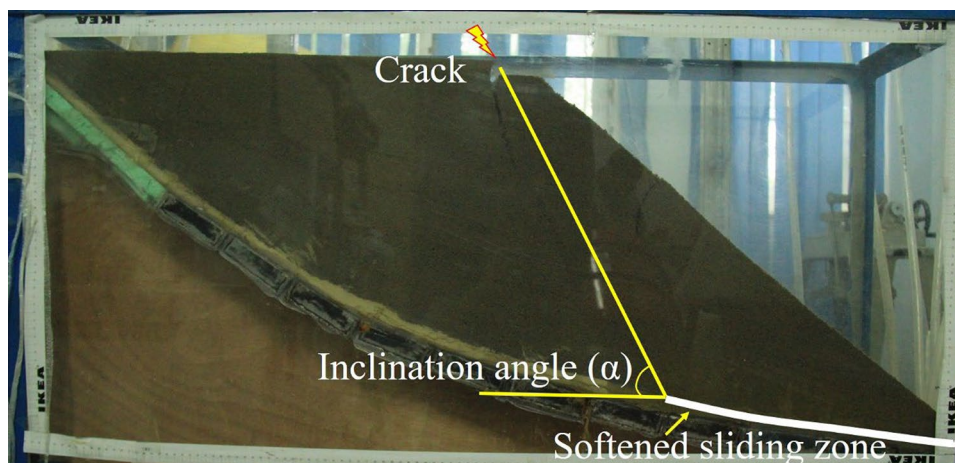**Fig. 14** Initial model of slope

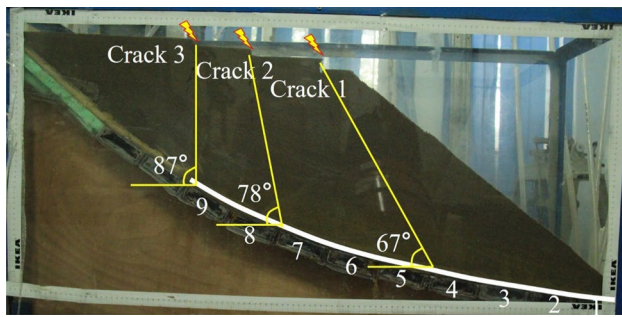**Fig. 15** Inclination angle α of the trailing edge fracture surface

Fig. 16 Inclination angles of the trailing edge fracture surfaces at all levels

Fig. 17 Generalization model of retrogressive landslides

The calculation method of inclination angles of trailing edge fracture surfaces

According to the evolution characteristics of the sliding masses of model slopes and the failure mode of the retrogressive landslides, the geomechanical model of the retrogressive landslides (Fig. 17) is generalized, and the inclination angles of the trailing edge fracture surfaces of sliding masses at all levels are calculated.

For the retrogressive landslides, the first-stage sliding mass is initially in a stable state. Due to the infiltration of surface water or the rise of groundwater, the shear strength of the sliding surface is reduced and gradually enters the limit equilibrium state. At this time, the shear strength of the sliding mass soil plays a role, bears a part of the shear force, and the damage continues to develop until the trailing edge fracture surface gradually penetrates the bottom sliding surface. The shear strength of the sliding mass is fully exerted; then, the sliding mass is unstable. Therefore, it is assumed that after the shear strength of the sliding zone soil is reduced to a certain value, the bottom sliding surface appears unstable sliding, and then, a tensile-shear failure surface is formed in
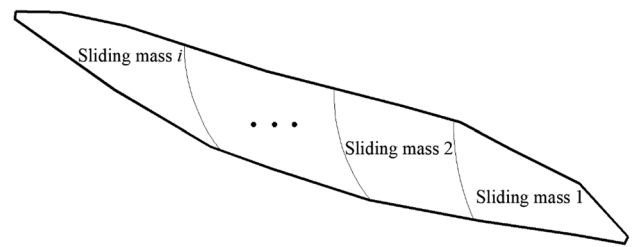
the sliding mass. Because the tensile stress value of soil is small, it cannot be calculated. At this time, only the safety factor of the bottom sliding surface is calculated, and the trailing edge fracture surface is in a critical state under the original shear strength parameters. According to the limit equilibrium condition and Mohr-Coulomb criterion, the equations are listed. By assuming the possible inclination angles of the trailing edge fracture surfaces when the sliding mass is destroyed, the safety factors of the sliding masses corresponding to different inclination angles are obtained. Finally, the inclination angle of the trailing edge fracture surface corresponding to the calculated minimum safety factor is the request (Sun et al. 2022). The specific solution process is shown in Fig. 18.
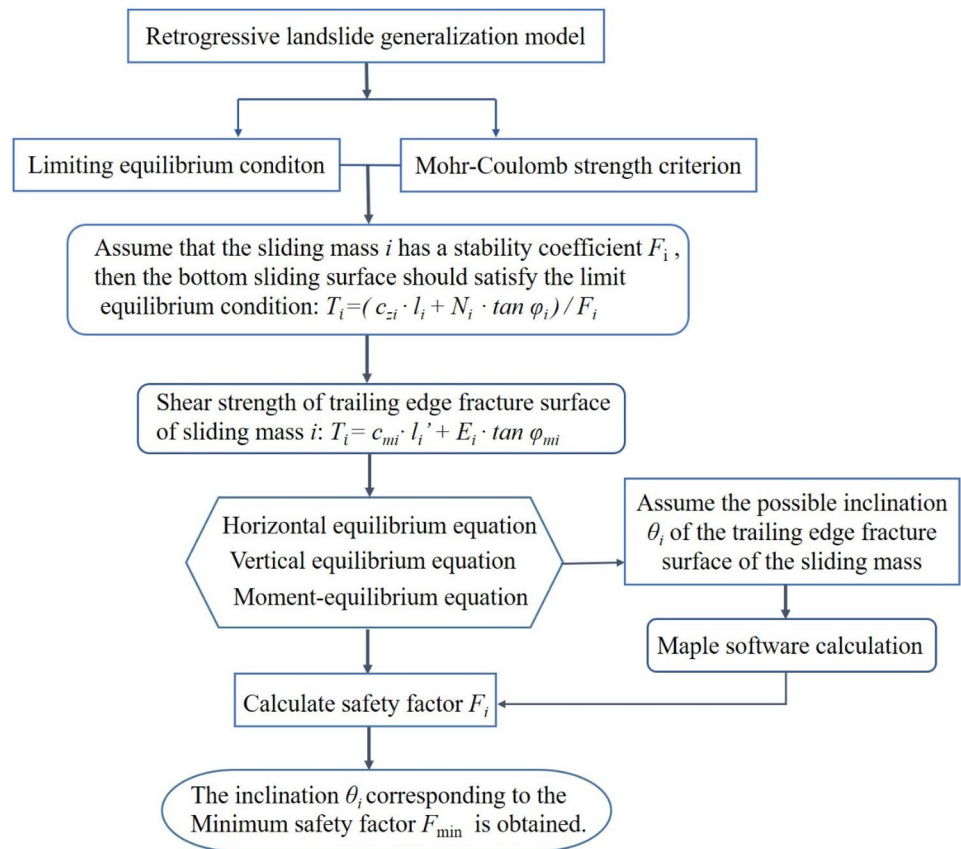
Mechanism analysis of trailing edge fracture surfaces

According to the existing slope stability analysis theory, it can be assumed that there are three possible formation mechanisms of the trailing edge fracture surfaces of retrogressive landslides: the overall sliding mechanism, the sliding tensile cracking mechanism, and the sliding shear deformation mechanism (Yang et al. 2018). Taking No. 1 as

Table 3 Test values of inclination angle α of the trailing edge fracture surfaces

No	GK$_1$	Inclination angle	GK$_2$	Inclination angle	GK$_3$	Inclination angle	GK$_4$	Inclination angle
1	2~3	80°	4~5	87°	6~7	78°	8~9	89°
2	2~4	76°	5~7	83°	8~10	72°		
3	2~5	79°	6~9	80°				
4	2~3	78°	4~5	75°	6~7	65°	8~9	77°
5	2~3	88°	4~5	88°	6~7	88°	8~9	88°
6	2~3	90°	4~5	90°	6~7	90°	8~9	84°
7	2~3	73°	4~5	67°	6~7	76°	8~9	75°
8	2~4	67°	5~7	78°	8~9	87°		
9	2~4	89°	5~7	86°	8~9	96°		
10	2~3	90°	4~5	99°	6~7	109°	8~9	103°
11	2~3	95°	4~5	103°	6~7	104°	8~9	81°
12	2~3	81°	4~5	72°	6~7	80°	8~9	81°

Fig. 18 The calculation process of the inclination angles of the trailing edge fracture surfaces

an example, the formation mechanism of the trailing edge fracture surfaces was discussed by comparing the calculation results of the three formation mechanisms with the experimental results.

The overall sliding mechanism

The overall sliding mechanism assumes that the sliding surfaces of retrogressive landslides are formed by combining the bottom sliding surfaces in the sliding zone soils and the trailing edge fracture surfaces in the sliding masses, both of which exert the shear strength simultaneously and have the same sliding safety factors.

The calculation model was established by using the two-dimensional rigid body limit equilibrium calculation software Rocscience Slide 5.0, and the known sliding surface was set according to the order of each working condition. For example, the permeation boxes of No. 1 were 2, 3, and 4, and then, the known sliding surface was shown in Fig. 19.

It is known that the search range of the inclination angles of the trailing edge fracture surfaces was set to $0 \sim 89°$ at the end of the sliding surfaces. When calculating, several trailing edge fracture surfaces were generated in the range of inclination search and combined with the bottom sliding surfaces to form the whole sliding surfaces. The safety factors of the sliding masses were calculated by the two-dimensional rigid body limit equilibrium method, and the fracture surfaces corresponding to the minimum safety factors were obtained. The calculation results were shown in Table 4.

It can be seen that the inclination angles of the fracture surfaces were generally $30° \sim 50°$. In the range of inclination search, the calculated values changed little and were far less than the experimental values.

The sliding tensile cracking mechanism

The formation mechanism of the trailing edge fracture surfaces is assumed that when the shear strength of the sliding zone soils decreases and the sliding masses slide forward, the trailing edge surfaces of the sliding masses appear tensile failure, and the trailing edge fracture surfaces are the tensile failure surfaces.

Therefore, the two-dimensional numerical calculation model was established, and the phase2 software (Abdollahipour and Rahmannejad 2013; Ghorbani et al. 2021) was used to

Fig. 19 Calculation model and results of rigid body limit equilibrium (unit: m)
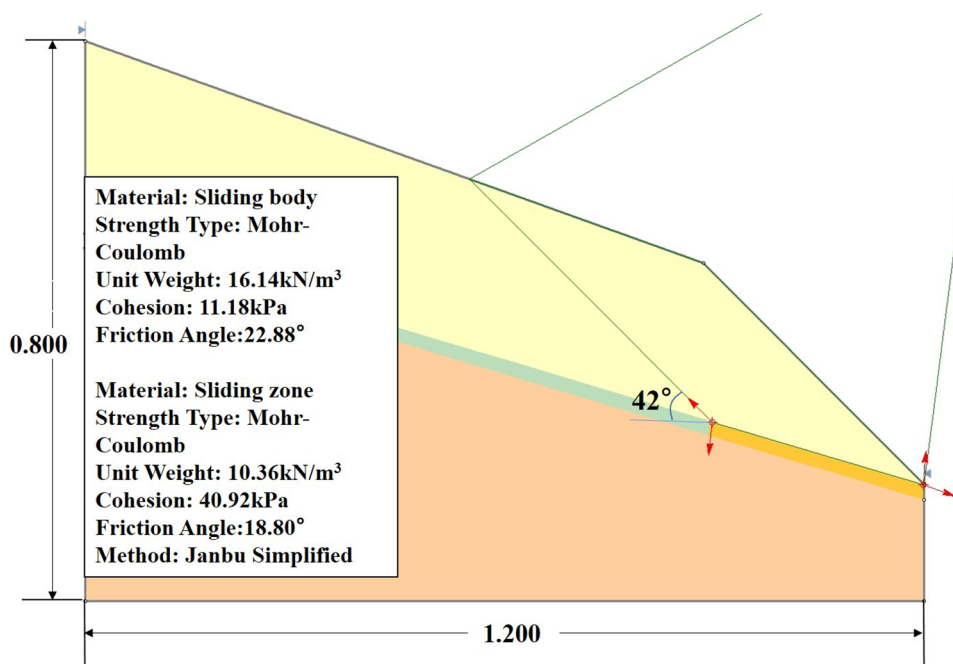
calculate the slope stress field. The shear strength parameters were selected according to the Table 2, and the Mohr-Coulomb ideal elastic-plastic constitutive model was adopted. Through software analysis, the maximum principal stress trace direction at the end of the permeable boxes under various working conditions was obtained, and the inclination angles of the trailing edge fracture surfaces were obtained, as shown in Fig. 20. The calculated values of the inclination angles were shown in Table 5.

It can be seen that the crack morphology of the trailing edge fracture surfaces shows a relatively consistent change rule with the test results, and the calculated inclination angles are also in good agreement with the test results.

The sliding shear deformation mechanism

Assuming that the sliding zone is unstable, the shear deformation occurs in the sliding mass, and the position of the maximum shear strain zone is the position of the trailing edge surface, which is controlled by the shear deformation.

A two-dimensional numerical calculation model was established, and the Phase2 software was used to calculate the maximum shear strain. The calculation parameters were shown in Table 2. To obtain a more obvious shear strain zone of the sliding mass, the water-saturated effect of the sliding zone soils was simulated by reducing the

Table 4 The comparison between the experimental values and the calculated values obtained by the overall sliding mechanism

No	GK1		GK2		GK3		GK4	
	Test value	Calculated value	Test value	Calculated value	Test value	Calculated value	Test value	Calculated value
1	80°	42°	87°	44°	78°	44°	89°	
2	76°	43°	83°	44°	72°			
3	79°	43°	80°					
4	90°	41°	89°	40°	92°	40°	79°	42°
5	88°	45°	88°	45°	88°	25°	84°	25°
6	90°	45°	90°	45°	90°	44°	84°	
7	78°	27°	78°	33°	76°	42°	75°	45°
8	67°	37°	78°	48°	87°	46°		
9	89°	41°	86°	47°	96°	48°		
10	90°	31°	99°	46°	109°	45°	103°	
11	95°	43°	103°	45°	104°	46°	81°	
12	81°	45°	72°	44°	80°	45°	81°	

Fig. 20 Principal stress vectors and the inclination angles of the trailing edge fracture surfaces (unit: m)
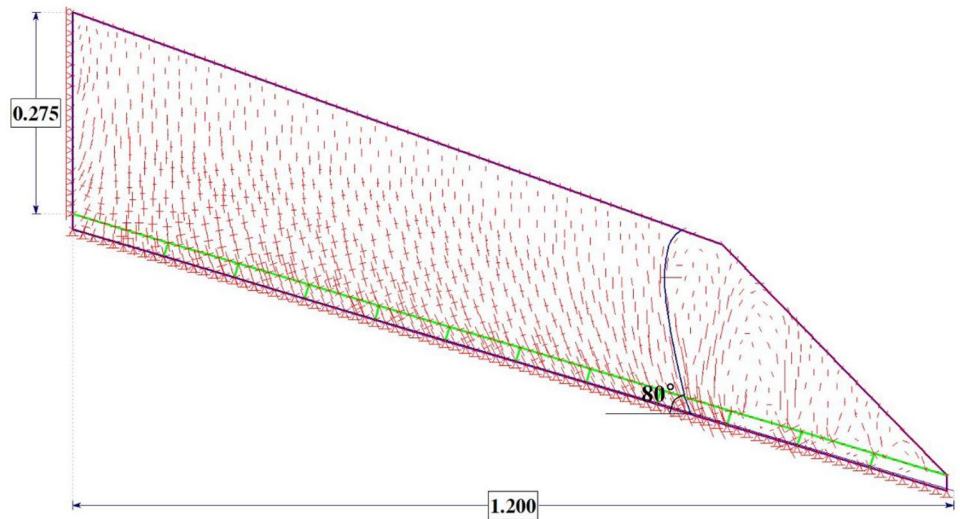
Table 5 The comparison between the experimental values and the calculated values obtained by the sliding tensile cracking mechanism

No	GK1		GK2		GK3		GK4	
	Test value	Calculated value	Test value	Calculated value	Test value	Calculated value	Test value	Calculated value
1	80°	80°	87°	84°	78°	79°	89°	90°
2	76°	78°	83°	89°	72°	80°		
3	79°	78°	80°	84°				
4	90°	87°	89°	89°	92°	89°	79°	84°
5	88°	82°	88°	89°	88°	86°	84°	83°
6	90°	92°	90°	82°	90°	83°	84°	84°
7	78°	83°	78°	84°	76°	83°	75°	89°
8	67°	67°	78°	88°	87°	94°		
9	89°	92°	86°	93°	96°	91°		
10	90°	92°	99°	100°	109°	100°	103°	97°
11	95°	92°	103°	105°	104°	98°	81°	108°
12	81°	99°	72°	99°	80°	94°	81°	93°

Fig. 21 Maximum shear strain concentration zone (unit: m)
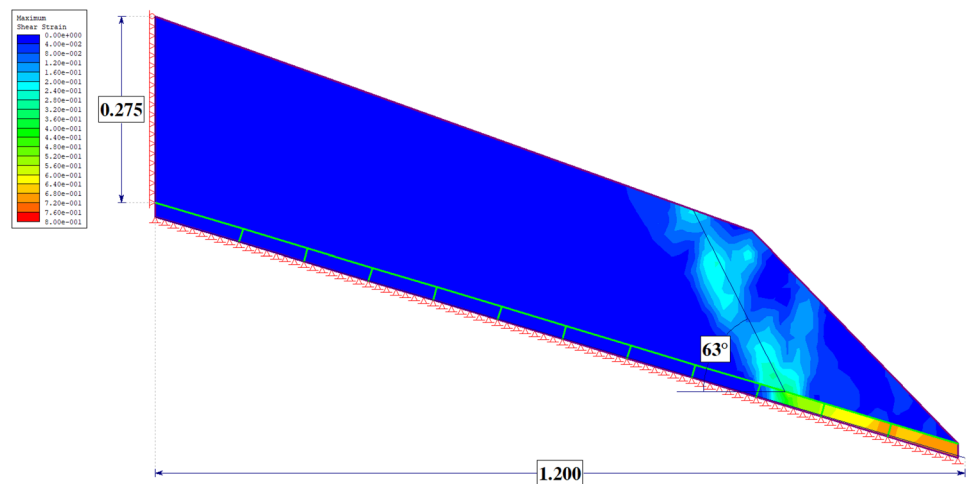
shear strength parameters of the sliding zone soils, and the cohesion and friction coefficient ($\tan\varphi$) of the sliding zone soils were both reduced to 30% of the natural values.

The calculation results showed that with the decrease in shear strength of the sliding zone soils, a prominent maximum shear strain concentration zone appeared in the sliding mass, as shown in Fig. 21. The midline of the shear strain concentration zone was determined, and the angle between it and horizontal plane was measured, which was the inclination angle of the trailing edge fracture surface (Table 6).

Discussion on formation mechanism of the trailing edge fracture surfaces

Analysis of calculation results of the inclination angles of the trailing edge fracture surfaces

This study mainly discusses the formation mechanism of the trailing edge surfaces from three aspects: the overall sliding mechanism, the sliding tensile cracking mechanism, and the sliding shear deformation mechanism. Comparing the calculation results of each mechanism with the model test, it is found that the calculated values of the overall sliding mechanism were much smaller than the experimental values, and the relative errors were more than 40%. The calculated values of the sliding shear deformation mechanism were relatively close to the experimental values, mostly smaller than the experimental values, and the relative errors were between 10% and 30%. The calculated values of the sliding tensile cracking mechanism were closest to the experimental values and fluctuated up and down the experimental values, and the relative errors were less than 10%.

Accordingly, it can be considered that the formation mechanism of the trailing edge surfaces of retrogressive landslides is due to the instability of the bottom sliding surface, a tensile failure zone appears at the sliding mass corresponding to the end of the unstable sliding surface. The tensile stress is controlled by the minimum principal stress, and the trailing edge tensile failure surface develops from the sliding surface to the slope surface. The direction of the tensile fracture surface is consistent with the direction of the maximum principal stress.

Formation mechanism analysis

The deformation and sliding of the landslides depend on the stress distribution and strength characteristics of the slope, and the stress distribution is related to the slope shapes, slope height, soil properties, and stratum distribution. In the deformation and the disintegration of retrogressive landslides, the exerting degree on the shear strength of rock and soil mass on the sliding surface is spatially inconsistent. The stress field of the landslides, especially the stress distribution and state of the sliding zone, has an important influence on the deformation and instability of the landslide body.

As a force system, the landslide body can be divided into an upper tension zone, a middle translation zone, and a lower resist-slip compression zone according to the stress characteristics. Affected by factors such as reservoir water level fluctuations and river erosion, the shear strength of the sliding zone at the slope toe decreases first, so the creep of the landslide body usually starts from the middle and lower parts, and the shear stress concentration is easy to form

Table 6 Comparison between the experimental values and the calculated values obtained by sliding shear deformation mechanism

No	GK1		GK2		GK3		GK4	
	Test value	Calculated value	Test value	Calculated value	Test value	Calculated value	Test value	Calculated value
1	80°	63°	87°	64°	78°	65°	89°	64°
2	76°	62°	83°	74°	72°	65°		
3	79°	64°	80°	68°				
4	90°	70°	89°	72°	92°	70°	79°	75°
5	88°	69°	88°	63°	88°	66°	84°	74°
6	90°	61°	90°	65°	90°	61°	84°	65°
7	78°	70°	78°	61°	76°	66°	75°	67°
8	67°	64°	78°	69°	87°	76°		
9	89°	63°	86°	69°	96°	62°		
10	90°	90°	99°	103°	94°	100°	103°	70°
11	95°	92°	103°	105°	104°	98°	81°	108°
12	81°	99°	72°	99°	80°	94°	81°	93°

near the foot of the slope due to sliding extrusion. When the shear stress of the sliding surface of the main sliding section exceeds its shear strength, creep occurs, the plastic zone is formed and gradually expanded, and the local slope creeps forward, which will lead to the active earth pressure failure of the rear stable slope due to the loss of lateral support force, forming the main tensile cracks of the landslides. Among them, the major principal stress σ_1 is the self-weight of the deformed sliding mass, and the small principal stress σ_3 is in the horizontal direction. Due to the decrease of σ_1, tension cracks in the vertical sliding direction are generated, forming the tension zone at the top of the slope. The larger the horizontal stress and the steeper the slope, the larger the tensile stress zone. With the extension and expansion of the tension cracks, the unstable sliding masses are gradually formed, and the landslide body undergoes creep-tension crack deformation.

Numerical models of PFC

The analysis is carried out using the particle flow program PFC^{2D} numerical simulation method (Wei et al. 2019; Wu et al. 2020; Zhang et al. 2021). This program has advantages in particle stability, deformation, and constitutive relationship. It can simulate the development process of large deformation of landslides and study the mechanical properties of landslides from a microscopic perspective. The evolution process and formation mechanism of the trailing edge cracks of the sliding masses are analyzed in the progressive failure process of the retrogressive landslides.

Due to the bonding parameters of different materials and the properties of the materials themselves being quite different, it is extremely important to calibrate the parameters of the materials before numerical simulation (Jiang et al. 2015; Xu et al. 2020). The specific step is to refer to the indoor experimental data and experience to give the numerical model a set of roughly estimated mesoscopic parameters, and then use the set of parameters to carry out the numerical experiment. According to the comparative analysis of the numerical experiment results and the indoor experiment results, if it exceeds the reasonable range, it is necessary to adjust the mesoscopic mechanical parameter model appropriately, and then carry out the simulation experiment again until the simulation experiment results are consistent with the indoor experiment results. This phenomenon shows that the set of mesoscopic parameters is reasonable and can be used for the next numerical simulation.

In this paper, the parameters were calibrated by the biaxial compression test, taking the No. 1 parameters as an example. The length of the numerical sample was 0.5 m and the height was 1.0 m, as shown in Fig. 22. The particle size was evenly distributed between 0.006 and 0.012 mm. The ratio of the longest edge L to the particle diameter d was
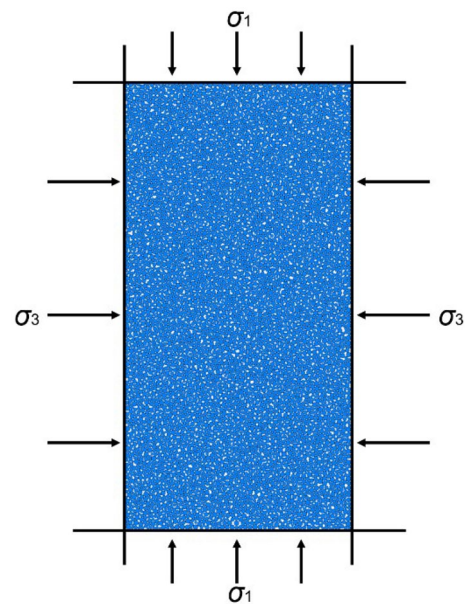

Fig. 22 Numerical model

about 111.11, which was larger than the ratio $L/d = 58$ determined by Jacobson. This indicated that the size was sufficient to form an obvious shear band. The normal stiffness was 1×10^8 N/m, and the tangential contact stiffness was 1.0×10^8 N/m, which was close to the literature values. The generation of samples was mainly divided into two stages. In the first stage, all particles were evenly placed within the sample range and there was no contact or overlap between any two particles. In the second stage, the friction force between particles was set to different specific values (0.45) to generate the initial sample. Then, the biaxial compression test was carried out. Control the stress to ensure that the confining pressure was reached before the partial load was implemented. Each sample was divided into four groups, and the confining pressure was 50 kPa, 100 kPa, 200 kPa, and 400 kPa, respectively.

The strength envelope of soil parameters was obtained by numerical test (Fig. 23). Based on this, the cohesion and internal friction angle of No. 1 sliding zone soil could be calibrated, which was consistent with the experimental data in this paper and could be used for subsequent simulation.

In the two-dimensional PFC^{2D} analysis model, the particles were simulated by a rigid disk, and the discrete particles transmitted force through contact. When the force acting on the contact point was greater than the contact strength, the particles would be separated, and the slope model would deform. The constitutive relationship of soil materials was mainly characterized by the micro-contact and bonding between particles. For homogeneous soil materials, more studies used the parallel bonding model to simulate. The particles under this model had normal strength, tangential

Fig. 23 Strength envelopes

$$c = 11.1 \text{ kPa}$$
$$\varphi = 31.4°$$
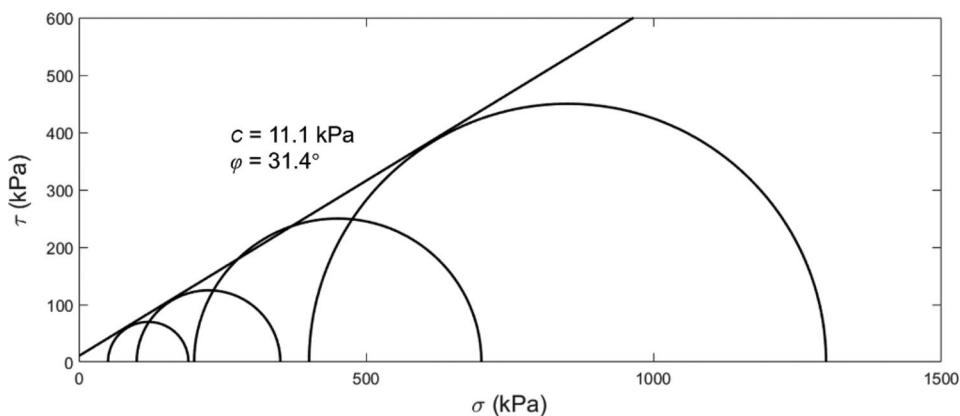
strength, normal stiffness, and tangential stiffness, and could resist tension, bending, and shear. Therefore, the parallel bond model was adopted to make the particles reach equilibrium under the self-weight conditions. The boundary of PFC was mainly set on the left and lower sides, both of which were rigid walls. In the PFC particle flow software, the generated particles could not pass through the wall by default, which was consistent with the boundary conditions of the model test. A numerical simulation of No. 1 was carried out using PFC^{2D}, and the analysis results were shown in Fig. 24.

Figure 24 showed the formation process of the trailing edge fracture surfaces, the deformation characteristics of the slope obtained by numerical simulation, the evolutionary morphology of cracks, and the contact force chain. It

could be seen from the apparent characteristics of the slope that the numerical simulation results were consistent with the model test results, indicating the effectiveness of the numerical simulation results. With the strength attenuation of each section of the sliding zone soil, the trailing edge cracks gradually formed in the landslide body, and the crack morphology was not single. There were arc, linear, folded lines, and other forms.

PFC^{2D} could simulate the fracture development process of soil particles. The normal bond failure between particles would lead to tensile failure of the slope, and the shear bond failure would cause shear failure. In the "Cracks" diagram, "green" represented the cracks generated by the tensile failure, and "blue" represented the cracks generated by the shear

Fig. 24 The progressive formation process of the trailing edge fracture surfaces using PFC^{2D}
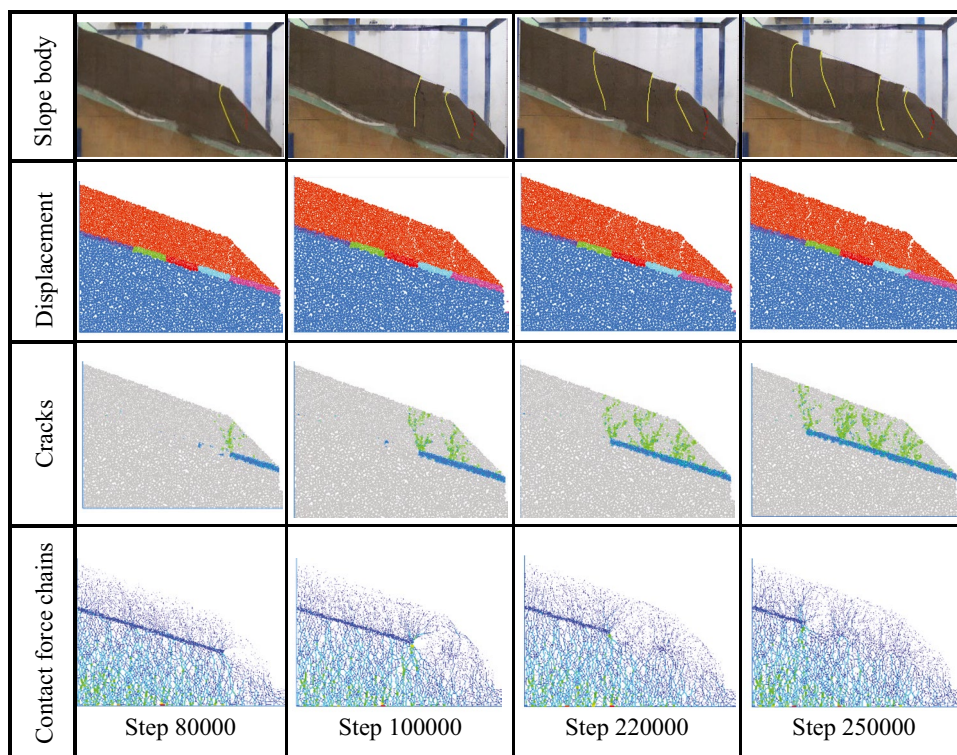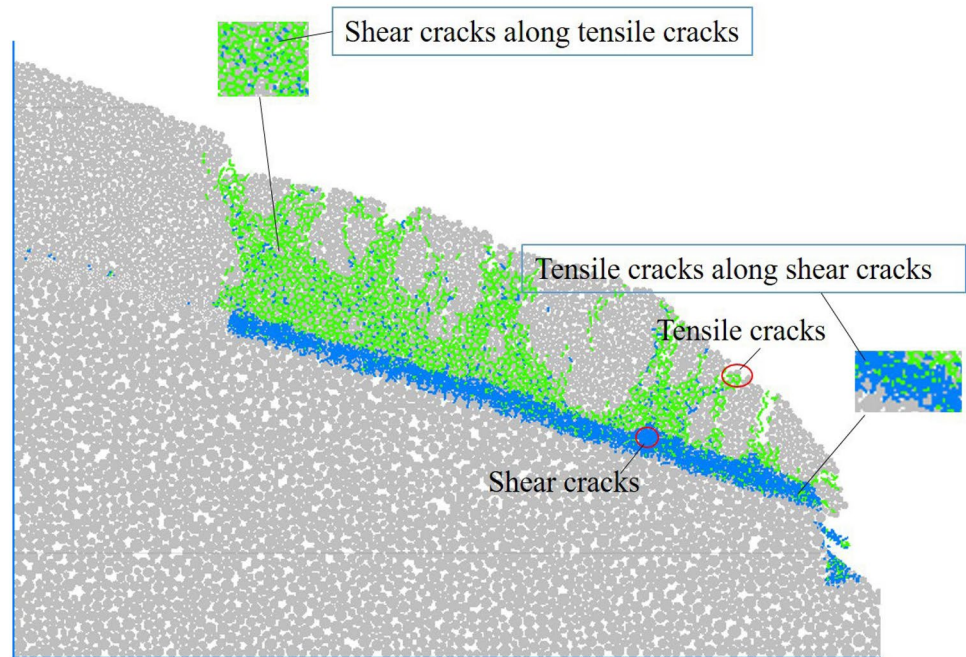
Fig. 25 Cracks development process

failure. It could be seen that with the instability of each sliding zone, the main crack would be generated inside the landslide, accompanied by the generation of some secondary cracks. With the increasing deformation of the sliding mass, the secondary cracks also developed, which stimulated the crack expansion and instability deformation inside the sliding mass. In the contact force chain contour, with the decrease of shear strength of the sliding zone soils, the connections between particles were gradually destroyed, and the deformed slope slid and lost the contact force until the final instability.

Figure 25 shows the instability characteristics of the retrogressive landslides. It can be seen that the sliding surface mainly occurs shear failure, accompanied by partial tensile failure, and the surface layer of the landslide body mainly undergoes tensile failure (Sun et al. 2023). With the deformation intensifies, the damage in the middle of the slope is still dominated by tensile failure, accompanied by shear failure, thus forming a tensile-shear mixed action zone. At this time, the normal bond and shear bond between particles are gradually destroyed until the whole landslide is unstable.

Conclusions

In this paper, the water-induced weakening retrogressive landslides were taken as the research objects, and the progressive failure process and formation mechanism of the trailing edge fracture surfaces were mainly analyzed by using the model test and numerical analysis method. The following conclusions were drawn:

1. There was a good correlation between the length of the unstable sliding zone and the deformation range of the slope. The longer the unstable sliding zone, the larger the deformation range of the slope body. An unstable sliding zone section corresponded to a single main crack, that was, when a certain sliding zone was unstable, only one main crack was observed on the slope corresponding to it.

2. The spatial forms of the trailing edge cracks inside the landslide body were mainly folded line, (inverted) arc, and linear type, and the fold-line cracks accounted for more than 1/2 of the total number. With the increase of slope thickness, the trailing edge cracks developed from "inverted arc" to "fold line" and finally presented a "straight line + half arc" type perpendicular to the slope. The increase of slope angles made the trailing edge cracks gradually transit from the "L" fold line perpendicular to the slope surface to the two fold lines, indicating that the slope failure gradually underwent translational failure and rotational failure until the two almost occurred simultaneously.

3. The inclination angles of the trailing edge fracture surfaces were mostly steep inclination angles of less than 90°, accounting for about 83.72% of the total. The inclination angles between 60° and 70° were about 6.98%, about 34.88% between 70° and 80°, and about 41.86% between 80 ° and 90 °. The inclination angles of the trailing edge fracture surfaces of the straight slope with equal thickness were parallel. The inclination angles of the trailing edge fracture surfaces increased with the increase of the slope thickness.

4. The calculated values of the sliding tensile cracking mechanism were closest to the experimental values, and the relative errors were less than 10%. The comprehensive analysis shows that the tensile failure plays a leading role in the formation of trailing edge fracture surfaces. Usually, the surface layer of the landslide is mainly subjected to tensile failure. The middle and lower parts of the slope are combined with a shear failure to form a mixed effect of tensile and shear, and the bottom sliding surface is mainly subjected to shear failure.

Declarations

Conflict of interest The authors declare no competing interests.

References

Abdollahipour A, Rahmannejad R (2013) Investigating the effects of lateral stress to vertical stress ratios and caverns shape on the cavern stability and sidewall displacements. Arab J Geosci 6:4811–4819. https://doi.org/10.1007/s12517-012-0698-z

Alimohammadlou Y, Najafi A, Gokceoglu C (2014) Estimation of rainfall-induced landslides using ANN and fuzzy clustering methods: a case study in Saeen Slope, Azerbaijan province. Iran Catena 120:149–162. https://doi.org/10.1016/j.catena.2014.04.009

Chang CY, Bo JS, Qi WH, Qiao F, Peng D (2022) Study on instability and damage of a loess slope under strong ground motion by numerical simulation. Soil Dyn Earthq Eng 152:107050. https://doi.org/10.1016/j.soildyn.2021.107050

Ding Y, Dang C, Yuan GX, Wang QC (2012) Characteristics and remediation of a landslide complex triggered by the 2008 Wenchuan, China earthquake—Case from Yingxiu near the earthquake epicenter. Environ Earth Sci 67:161–173. https://doi.org/10.1007/s12665-011-1489-7

Eshraghian A, Martin CD, Morgenstern NR (2008) Movement triggers and mechanisms of two earth slides in the Thompson River Valley, British Columbia, Canada. Can Geotech J 45:1189–1209. https://doi.org/10.1139/T08-047

Ghorbani E, Moosavi M, Hossaini MF, Assary M, Golabchi Y (2021) Determination of initial stress state and rock mass deformation modulus at Lavarak HEPP by back analysis using ant colony optimization and multivariable regression analysis. Bull Eng Geol Env 80:429–442. https://doi.org/10.1007/s10064-020-01936-2

Graber A, Santi P, Arestegui PM (2021) Constraining the critical groundwater conditions initiation of large, irrigation-induced landslides, Siguas River Valley, Peru. Landslides 18:3753–3767. https://doi.org/10.1007/s10346-021-01767-6

Guo C, Zhang Y, Li X, Ren S, Yang Z, Wu R, Jin J (2020) Reactivation of giant Jiangdingya ancient landslide in Zhouqu County, Gansu Province, China. Landslides 17:179–190. https://doi.org/10.1007/s10346-019-01266-9

Huang D, Gu DM, Song YX, Cen DF, Zeng B (2018) Towards a complete understanding of the triggering mechanism of a large reactivated landslide in the Three Gorges Reservoir. Eng Geol 238:36–51. https://doi.org/10.1016/j.enggeo.2018.03.008

Huang D, Luo SL, Zhong Z, Gu DM, Song YX, Tomás R (2020) Analysis and modeling of the combined effects of hydrological factors on a reservoir bank slope in the Three Gorges Reservoir area. China Eng Geol 279:105858

Hu XD, Zhang L, Hu KH, Cui L, Wang L, Xia ZY (2022) Modelling the evolution of propagation and runout from a gravel-silty clay landslide to a debris flow in Shaziba, southwestern Hubei Province, China. Recent Landslides 19:2199–2212. https://doi.org/10.1007/s10346-022-01897-5

Jiang MJ, Jiang T, Crosta GB, Shi ZM, Chen H, Zhang N (2015) Modeling failure of jointed rock slope with two main joint sets using a novel DEM bond contact model. Eng Geol 193:79–96. https://doi.org/10.1016/j.enggeo.2015.04.013

Jiang Q, Cui J, Feng XT, Jiang YJ (2014) Application of computerized tomographic scanning to the study of water-induced weakening of mudstone. Bull Eng Geol Env 73:1293–1301. https://doi.org/10.1007/s10064-014-0597-5

Kaya A, Akgiin A, Karaman K, Bulut F (2016) Understanding the mechanism of slope failure on a nearby highway tunnel route by different slope stability analysis methods: a case from NE Turkey. Bull Eng Geol Env 75:945–958. https://doi.org/10.1007/s10064-015-0770-5

Kennedy R, Take WA, Siemens G (2021) Geotechnical centrifuge modelling of retrogressive sensitive clay landslides. Can Geotech J 58:1452–1465. https://doi.org/10.1139/cgj-2019-0677

Lian B, Peng J, Zhan H, Huang Q, Wang X, Hu S (2020) Formation mechanism analysis of irrigation-induced retrogressive loess landslides. Catena 195:104441. https://doi.org/10.1016/j.catena.2019.104441

Liao K, Wu Y, Miao F, Li L, Xue Y (2021) Effect of weakening of sliding zone soils in hydro-fluctuation belt on long-term reliability of reservoir landslides. Bull Eng Geol Env 80:3801–3815

Liu B, Wang CK, Liu ZY, Xu ZH, Nie LC, Pang YH, Wang N, Feng SX (2021) Cascade surface and borehole geophysical investigation for water leakage: a case study of the Dehou reservoir, China. Eng Geol 294:1–12. https://doi.org/10.1016/j.enggeo.2021.106364

Liu F, Li J (2015) Landslide erosion associated with the Wenchuan earthquake in the Minjiang River watershed: implication for landscape evolution of the Longmen Shan, eastern Tibetan Plateau. Nat Hazards 76:1911–1926. https://doi.org/10.1007/s11069-014-1575-8

Li AJ, Mburu JW, Chen CW, Yang KH (2022) Investigations of silty soil slopes under unsaturated conditions based on strength reduction finite element and limit analysis. KSCE 26(3):1095–1110. https://doi.org/10.1007/s12205-021-1162-y

Lv H, Ling C, Hu B, Ran J, Zheng Y, Xu Q, Tong J (2019) Characterizing groundwater flow in a translational rock slide of southwestern China. Bull Eng Geol Environ 78:1989–2007. https://doi.org/10.1007/s10064-017-1212-3

Oezdemir A, Delikanli M (2009) A geotechnical investigation of the retrogressive Yaka Landslide and the debris flow threatening the town of Yaka (Isparta, SW Turkey). Nat Hazards 49:113–136. https://doi.org/10.1007/s11069-008-9282-y

Pan YH, Chen JP, Wu LQ, Wang W, Tan FL (2017) Evolution mechanism and rainfall warning criteria for Maijianwo slope in Henan Province, China. Geotech Geol Eng 35:183–194

Qi X, Xu Q, Liu F (2018) Analysis of retrogressive loess flowslides in Heifangtai, China. Eng Geol 236:119–128. https://doi.org/10.1016/j.enggeo.2017.08.028

Regmi RK, Jung K, Nakagawa H, Kang J (2014) Study on mechanism of retrogressive slope failure using artificial rainfall. CATENA 122:27–41. https://doi.org/10.1016/j.catena.2014.06.001

Shan Z, Zhang W, Wang D, Wang L (2021) Numerical investigations of retrogressive failure in sensitive clays: revisiting 1994 Sainte-Monique slide, Quebec. Landslides 18:1327–1336. https://doi.org/10.1007/s10346-020-01567-4

Skempton AW (1964) Long-term stability of clay slopes. Geotechnique 14(2):77–102

Su X, Wei WH, Ye WL, Meng XM, Wu WJ (2019) Predicting landslide sliding distance based on energy dissipation and mass point kinematics. Nat Hazards 96:1367–1385. https://doi.org/10.1007/s11069-019-03618-z

Sun LJ, Li CJ, Shen FM (2022) Two-surface progressive failure mechanism and stability quantitative evaluation of water-induced weakening retrogressive landslides: case study for clay landslides. China Bull Eng Geol Env 81:382. https://doi.org/10.1007/s10064-022-02860-3

Sun LJ, Li CJ, Shen FM, Zhang HZ (2023) Reactivation mechanism and evolution characteristics of water softening-induced reservoir-reactivated landslides: a case study for the Three Gorges Reservoir Area, China. Bull Eng Geol Env 82:66. https://doi.org/10.1007/s10064-023-03084-9

Sun L, Yang T, Cheng Q, Wu D (2018) Experimental study on couse of progressive formation of retrogressive landslide. J Southwest Jiaotong Univ 53:762–771 (in Chinese)

Take WA, Beddoe RA, Davoodi-Bilesavar R, Phillips R (2015) Effect of antecedent groundwater conditions on the triggering of static liquefaction landslides. Landslides 12:469–479. https://doi.org/10.1007/s10346-014-0496-7

Troncone A, Conte E, Donato A (2015) Two and three-dimensional numerical analysis of the progressive failure that occurred in an excavation-induced landslide. Eng Geol 183:265–275. https://doi.org/10.1016/j.enggeo.2014.08.027

Wang B, Vardon PJ, Hicks MA (2016) Investigation of retrogressive and progressive slope failure mechanisms using the material point method. Comput Geotech 78:88–98. https://doi.org/10.1016/j.compgeo.2016.04.016

Wang Q, Wang Z, Su Y, Zhong X, Wang L, Ma H, Zhang G, Woolery EE, Liu K (2020) Characteristics and mechanism of the landslide in Yongguang village, Minxian County, China. Nat Hazards 105:1413–1438. https://doi.org/10.1007/s11069-020-04360-7

Wei JB, Zhao Z, Xu C, Wen Q (2019) Numberical investigation of landslide kinetics for the recent Mabian landslide (Sichuan, China). Landslides 16:2287–2298. https://doi.org/10.1007/s10346-019-01237-0

Wu ZJ, Zhang D, Wang SN, Liang C, Zhao DY (2020) Dynamic-response characteristics and deformation evolution of loess slopes under seismic loads. Eng Geol 267:105507. https://doi.org/10.1016/j.enggeo.2020.105507

Xu L, Dai FC, Chen J, Iqbal J, Qu YX (2014) Analysis of a progressive slope failure in the Xiangjiaba reservoir area, Southwest China. Landslides 11:55–66. https://doi.org/10.1007/s10346-012-0373-1

Xu R, Liu EL, Jiang XQ, Tian JQ, Sun Y (2020) Analysis on evolution of mesostructure of cohesionless soil ground upon loading. Powder Technol 368:1–13. https://doi.org/10.1016/j.powtec.2020.04.048

Xu X, Guo WZ, Liu Y, Ma J, Wang W, ZhangH GH (2017) Landslides on the loess plateau of China: a latest statistics together with a close look. Nat Hazards 86:1393–1403. https://doi.org/10.1007/s11069-016-2738-6

Yang T, Sun LJ, Cheng QH, Zhong W (2018) Experimental study on formation mechanism of the trailing edge failure surface of retrogressive landslide. CJRME 37(Supp2):3842–3849

Yin YP, Huang BL, Zhang Q, Yan GQ, Dai ZW (2020) Research on recently occurred reservoir-induced Kamenziwan rockslide in Three Gorges Reservoir, China. Landslides 17:1935–1949. https://doi.org/10.1007/s10346-020-01394-7

Zhang KQ, Wang LQ, Zhang WG, Zhang ZH, Zhou H (2021) Formation and failure mechanism of the Xinfangzi landslide in Chongqing city (China). Appl Sci 11:8963. https://doi.org/10.3390/app11198963

Zhang LF, Wu YP, Miao FS, Li LW, Kang T (2020) Mechanical model and stability analysis of progressive failure for thrust-type gently inclined shallow landslide. Rock Soil Mech 40(12):4767–4776. https://doi.org/10.16285/j.rsm.2018.1885

Zhang S, Xu Q, Hu ZM (2016) Effects of rainwater softening on red mudstone of deep-seated landslide, Southwest China. Eng Geol 204:1–13. https://doi.org/10.1016/j.enggeo.2016.01.013

Zuo S, Zhao LH, Deng DP, Han Z, Zhao B, Zhao ZG (2021) Back analysis of shear strength parameters for progressive landslides: case study of the Caifengyan landslide. China Bull Eng Geol Env 81(1):19. https://doi.org/10.1007/s10064-021-02507-9